

## Vegetation monitoring in refugee-hosting areas in South Sudan

Reik Leiterer<sup>a,\*</sup>, Urs Bloesch<sup>b</sup>, Hendrik Wulf<sup>a</sup>, Sebastian Eugster<sup>c</sup>, Philip Claudio Joerg<sup>a</sup>

<sup>a</sup> Remote Sensing Laboratories, Department of Geography, University of Zurich, Winterthurerstrasse 190, CH-8057, Zurich, Switzerland

<sup>b</sup> Adansonia-Consulting, Chemin de Malvaux 4, CH-2533, Evilard, Switzerland

<sup>c</sup> Swiss Agency for Development and Cooperation, Effingerstrasse 27, CH-3003, Bern, Switzerland

### ARTICLE INFO

#### Keywords:

Environmental impact  
Natural resources management  
Humanitarian operation  
Earth Observation  
Remote sensing  
Vegetation mapping

### ABSTRACT

Mass population displacements put additional stress on the ecosystems and often lead to conflicts with the host communities, especially in the case of large refugee or Internally Displaced Person (IDP) camps. Therefore, there is need for the assessment of environmental impacts and, based on this, the sustainable management of natural resources between host and refugee communities. We propose a method based on high (Landsat 5, 7 and 8) and very high (WorldView-2) resolution Earth Observation data to establish forest inventories combining the analysis of remote sensing satellite data along with ground-based observations in South Sudan. The resulting forest inventory mapping comprises map products on vegetation cover, tree species, and vegetation changes. We distinguished between the vegetation types grassland, shrub/tree savanna, savanna woodland, and woodland. For savanna woodland and woodland, we furthermore applied a tree species classification, differentiating between Red acacia, Desert date tree, Silak, and Doum palm. The tree species classification yielded in mean accuracies of about 61.0% for both the Landsat and WorldView based classifications, with the best results achieved for Desert palm tree and red acacia with average accuracies of 88% and 53%, respectively. The product about vegetation changes indicates a decrease of vegetation up to 50% within and in the surroundings of the refugee camps/settlement. The resulting maps can serve to estimate accessible wood resources and to identify potential harvest areas. In addition, they can support the definition of a sustainable use of wood for construction and cooking purposes for the refugee and host communities based on a community forest management.

### 1. Introduction

High levels of environmental degradation often stem from the dependency of highly concentrated populations upon natural resources including water, agricultural land, pastures, and forests (Foley et al., 2011; Raleigh & Urdal, 2007; Tschamtket et al., 2012). Mass population displacements put additional stress on the ecosystems especially in the case of large refugee or IDP (Internally Displaced Person) camps (Kranz, Sachs, & Lang, 2015; Spröhnle, Kranz, Schoepfer, Moeller, & Voigt, 2016). By the end of 2015, 65.3 million individuals were forcibly displaced worldwide because of persecution, conflict, generalized violence, or human rights violations (UNHCR, 2016). Weak environmental governance and the fact that displaced communities often compete for the same dwindling natural resources as the local communities exacerbates the risk of new conflicts [cf. (Lyytinen, 2009; Oshiek, 2015; Raleigh & Urdal, 2007; Thulstrup & Henry, 2015; UNEP, 2009)].

The additional needs of displaced communities for both firewood and charcoal (hereafter fuelwood) for cooking, heating and lighting purposes (Spröhnle et al., 2016) as well as their demand for shelter

building material are often not addressed in a comprehensive and timely manner in the humanitarian response (Thulstrup & Henry, 2015; UNHCR, 2014). The resulting deforestation, often accelerated by commercial activities such as wood trade, charcoal making, or the fuel-intensive brick-making (Abdelsalam, 2014, pp. 89–106; Alam & Starr, 2009; Bloesch, Schneider, & Lino, 2013) may lead to long-lasting environmental impacts thereby affecting the resilience of the host communities largely depending on intact natural resources (Salih, Körnich, & Tjernström, 2013; UNEP, 2007).

A forest mapping and inventory has been recommended for the Sudanese refugee-hosting areas in the northern South Sudan by a UNHCR (United Nations High Commissioner for Refugees) environmental inception mission (Bloesch et al., 2013). Traditionally, forest mapping and inventory is carried out by fieldwork in relatively small sampling areas, which is time consuming and occasionally subjective (Foody, 2010; Haara & Leskinen, 2009; McElhinny, Gibbons, Brack, & Bauhus, 2005). In South Sudan, however, the vast areas and distances as well as difficulties of access because of the security situation make traditional forest mapping infinitely more complex (Gorsevski, Geores, &

\* Corresponding author. Remote Sensing Laboratories, Department of Geography, University of Zurich, Winterthurerstrasse 190, CH-8057, Zurich, Switzerland.

E-mail addresses: [reik.leiterer@geo.uzh.ch](mailto:reik.leiterer@geo.uzh.ch) (R. Leiterer), [bloesch@swissonline.ch](mailto:bloesch@swissonline.ch) (U. Bloesch), [hendrik.wulf@geo.uzh.ch](mailto:hendrik.wulf@geo.uzh.ch) (H. Wulf), [sebastian.eugster@eda.admin.ch](mailto:sebastian.eugster@eda.admin.ch) (S. Eugster), [philip.joerg@geo.uzh.ch](mailto:philip.joerg@geo.uzh.ch) (P.C. Joerg).

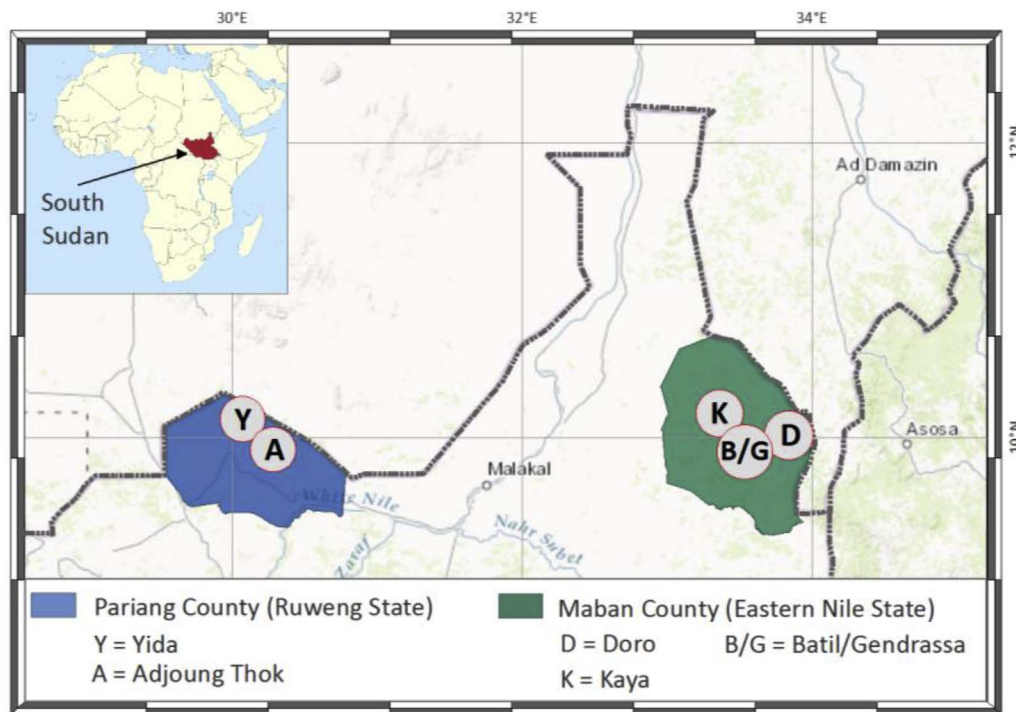


Fig. 1. Overview of the refugee camps/settlement in the counties Pariang and Maban.

Kasischke, 2013; UNESCO, 2013). Earth Observation (EO) can therefore be a good alternative to remotely map and characterize woody formations over large areas following objective criteria (Banskota et al., 2014; Mbow, Fensholt, Nielsen, & Rasmussen, 2014; Roberts, Tesfamichael, Gebreslasie, Van Aardt, & Ahmed, 2007; Tomppo et al., 2008).

For generally rather open woody formations such as occurring in northern South Sudan, high and very high resolution EO data are very suitable to map and characterize these formations [cf. (Boggs, 2010; Gara, Murwira, Ndaimani, Chivhenge, & Hatendi, 2015; Gorsevski et al., 2013; Zeidler, Wegmann, & Dech, 2012)]. EO data with high resolution (HR) are defined by spatial resolution of about tens of meters; whereas EO data with very high resolution (VHR) are defined by a spatial resolution of about 1 m (Moeller et al., 2011). There are few studies in which this kind of open woody formations and their changes have been studied supported by using high resolution EO data, including both quantitative methods and visual interpretation [e.g. (Gonzalez, Tucker, & Sy, 2012; Gorsevski, Kasischke, Dempewolf, Loboda, & Grossmann, 2012; Herrmann & Tappan, 2013; Mbow et al., 2014)]. In addition, very high resolution data were used for identification of individual trees and detailed monitoring of changes in woody cover and standing stock [e.g. (Kelder, Nielsen, & Fensholt, 2013; Rasmussen et al., 2011; Tiede et al., 2009; Wu, De Pauw, & Helldén, 2013)]. Gorsevski et al. (2012, 2013), for example, investigated the changes in land cover as well as implications for forested areas (in terms of *no change*, *loss* and *gain* of forests) during civil unrest in South Sudan. However, the authors concluded that the study was only conducted on a very minimal scale and based mainly on HR satellite data (Landsat TM and ETM+), whereby VHR data were solely used for validation purposes.

In contrast, Lang, Tiede, Hölbling, Füreder, and Zeil (2010) used multi-temporal, VHR satellite data (QuickBird) for an automatic analysis of IDP camp evolution in Darfur, but rather focused on camp's outlines and inner structure. Also, using multi-temporal QuickBird data but with stronger focus on the environmental impacts, Hagenlocher, Lang, and Tiede (2012) analysed the relationship between land cover and land cover changes and the increasing IDP camp population in Sudan. The sole use of VHR data, however, hinders an assessment of

environmental impacts on larger scale. Moreover, the availability of this kind of data is limited and highly depends on the acquisition requests in the past (usually you rarely find more than 1 acquisition per year in these regions) and the data procurement itself often involves high costs (i.e. tasking new data acquisitions). Kranz et al. (2015) assessed environmental changes in Darfur induced by IDP camps on a regional scale based on free available, multi-temporal EO data of the medium resolution spectrometer MODIS. This resolution, however, would not allow an accurate estimate of wood resources for the Sudanese refugees and host communities and the identification and mapping of the dominant tree species at large scale what is a novelty of this study. In addition, another factor that is decisive for the characterization of vegetation in those areas must be considered: the temporal scale, i.e. the phenology of the vegetation (Brandt et al., 2017; Horion, Fensholt, Tagesson, & Ehammer, 2014; Symeonakis & Higginbottom, 2014). The vegetation adapts to the annual cycle of rainfall with a slight temporal delay, whereby during the long drought some parts of the vegetation withers and shows no photosynthetic activity until the next rainfall (Asner & Heidebrecht, 2002). Therefore, an important issue for the characterization of vegetation types is the use of multi-temporal data, which should be taken between the end of the rainy season and the end of the dry season [cf. (Cissé et al., 2016; Hahn-Hadjali & Schmid, 1999; Liu, Heiskanen, Aynekulu, & Pellikka, 2015)].

Thus, we propose a multi-scale and multi-temporal EO approach to derive not only the primary land cover classes and their changes but also the dominant tree species on a regional scale. The aim of this paper is i) to classify the main vegetation types for the refugee-hosting areas in northern South Sudan using multi-scale EO data, ii) to further distinguish savanna woodland and woodland based on the dominant tree species – having each a specific purpose of use [cf. (Bloesch et al., 2013)], iii) to assess changes in forest cover and thus to estimate the impact of the Sudanese refugee camps/settlement on the local ecosystems, and iv) to discuss the replication potential of the methodology for humanitarian operations. The resulting vegetation maps serve as a basis to estimate the total amount of accessible wood resources, identify potential harvest areas, and support the definition of a sustainable use of poles and fuelwood for the refugee and host communities based on a

community forest management.

## 2. Study sites

Since July 2011 fighting in the Sudanese states of South Kordofan and Blue Nile led to the escape of about 200,000 people to South Sudan (Alam & Starr, 2009). UNHCR started his emergency response in September 2011 by setting up refugee camps in the former Pariang County (9°56' N, 30°35' E) in Ruweng State (formerly Unity State) and the former Maban County (9°58' N, 33°45' E) in Eastern Nile State (formerly Upper Nile State) (Fig. 1) (Salih et al., 2013; UNESCO, 2013).

Further escalating violence in South Sudan during December 2013 displaced more than 1 million people internally and led to the arrival of new refugees in these camps (Bloesch, 2014). Given the sparse population of ca. 82,000 and 36,000 inhabitants in the counties Pariang and Maban (Tiller & Healy, 2013), the refugees are with approx. 83,000 and 126,000 persons outnumbering the local host communities (Bloesch, 2014). The permanent need of the refugees for building materials (wooden poles and sticks) for shelter and latrines as well as for their daily domestic energy consumption (cooking, heating and lighting) led to rapid deforestation around the refugee camps/settlement. The radius of deforestation around the refugee camps/settlement is steadily increasing, whereby the cutting rate decreases with increasing distance from the refugee camps/settlement. Moreover, the deforestation is greatly accelerated by illegal charcoal making facilitated by the new all-weather roads built for the humanitarian operation. The impact on the local ecosystems is thus significant in the surroundings of the refugee camps/settlement with an inherent conflict potential with the host communities (Bloesch et al., 2013). For more details on the socio-political context and the biogeography of the Sudanese refugee hosting areas we refer to Bloesch et al. (2013) and Ndegwa (2016).

The rainfall regime in Pariang and Maban is unimodal with a single rainy season from May to October (Chen, Guo, Zhang, & Xu, 2013; Sosnowski, Ghoneim, Burke, Hines, & Halls, 2016). According to Climate-data.org (Climate-date, 2017) and Chen et al. (2013) mean annual rainfall is ranging between 500 mm and 800 mm. Strong variations in seasonal precipitation lead often to local and area-wide flooding and drought (Zhang, Xu, Yong, Hu, & Sun, 2012). Extensive inundation in the rainy season is a normal phenomenon on the flat flood plains, whereas most rivers and streams exist solely during the rainy season. Temperatures are hot in the dry season, often exceeding 45 °C in February and March, with extremely low humidity levels (Maystadt, Calderone, & You, 2015).

Following the nomenclature of the *Yangambi* classification [cf. (C.S.A., 1956)], the vegetation types in the Sudanese refugee-hosting areas mainly comprise woodlands, savanna woodlands, tree/shrub savannas, grasslands, and few narrow pockets of riverine forests mainly along the permanent Yabus River in Maban County. The dominating tree species are Red acacia (*Acacia seyal*), Dessert date tree (*Balanites aegyptiaca*), Silak (*Anogeissus leiocarpus*), and Doum palm (*Hyphaene thebaica*), which all may form virtually monospecific tree stands (Bloesch et al., 2013). Each of this species has a specific purpose of use (cf. Table 1) and is of utmost importance for the local communities [cf. (Bloesch, 2014)].

Most vegetation types, however, contain next to green vegetation also dried up vegetation that is known as non-photosynthetic vegetation (NPV) (Asner & Heidebrecht, 2002). NPV is dormant and photosynthetically inactive during the dry season that lasts approximately from November to April.

## 3. Data and methods

### 3.1. Data

#### 3.1.1. Earth Observation data

For the multi-scale EO approach high resolution data from the

**Table 1**  
The dominant tree species considered and their specific purpose of use.

Tree species	Purpose of use
Red acacia	- Food source for livestock, fuelwood/charcoal, small-scale constructions, medicinal uses
Desert date tree	- Food source/famine food, furniture, durable items (tools), fuelwood/charcoal, medicinal uses
Silak	- Piles and rafters in house construction, durable items (tools), furniture, carving, fuelwood/charcoal, lye for washing, medicinal uses
Doum palm	- Basket making, ropes and strings, piles and rafters in house construction, furniture, food source

Landsat missions (Landsat 5, 7 and 8) (Irons, Dwyer, & Barsi, 2012) and VHR data from WorldView-2 (Immitzer, Atzberger, & Koukal, 2012) were available (Fig. 2).

Landsat data were downloaded via the *EarthExplorer* web-portal (<http://earthexplorer.usgs.gov/>), whereas WorldView-2 data were provided by the Operational Satellite Applications Programme (UNOSAT) of the United Nations Institute for Training and Research. The EO dataset comprise 6 WorldView-2 and 81 Landsat imagery. The data selection generally aimed at obtaining images with minimum cloud cover on different times of the dry season (November–April) and the rainy season (May–October). All WorldView-2 scenes were acquired in April, November and December 2013 and cover all the refugee camps/settlements in Maban county. A temporal overview of the used Landsat images is given in Fig. 3.

Pariang and Maban are covered in each case by one Landsat tile (Pariang: path 174/row 53, Maban: path 172/row 53). WorldView-2 data were available only for Maban, whereby a full coverage of the refugee camps and the surroundings was ensured but not for the whole area of the county.

The Landsat and WorldView-2 data were calibrated and converted to top-of-atmosphere spectral radiance and reflectance to enable spectral analyses (Updike and Comp., 2010). Radiometric calibration is a common pre-processing step to compensate for radiometric errors from sensor defects, variations in scan angle, and system noise to produce an image that represents true spectral radiance at the sensor [cf. (Chander, Markham, & Helder, 2009; Crespi & de Vendictis, 2009; Pu, Landry, & Zhang, 2015)]. For WorldView-2, we employed the radiometric calibration using the software programs ArcGIS<sup>®</sup>, ENVI<sup>®</sup> and Matlab<sup>®</sup>, following the method described by Updike and Comp. (2010). The pre-processing of the Landsat data was implemented using the established preprocessing tools in ENVI<sup>®</sup> (version 5.1).

Even we applied a pan-sharpening for achieving higher spatial resolutions for both the Landsat and WorldView images, the pan-sharpened images were only used visually for the identification of suitable field plots for ground truth measurements (cf. chapter 3.1.2), as pan-sharpening not necessarily improves the spectral information content we focused on with our classification approach.

For Landsat-7, artefacts in the images introduced by the failure of the Scan Line Corrector, compensating for the forward motion of satellite [cf. (Chen, Zhu, Vogelmann, Gao, & Jin, 2011)], were masked out. Furthermore, data gaps introduced by clouds and clouds shadows, which mask or alter the spectral response of the underlying land cover, were also masked out. We used the software *Fmask* (Function of mask) as stand-alone version and implemented in MATLAB<sup>®</sup> to detect and mask clouds and associated cloud shadow regions in Landsat imagery (Jabar, Sulong, & George, 2014; Zhu, Liu, & Chen, 2012). For a better discrimination of vegetation from its surrounding and non-photosynthetic vegetation, we calculated for each Landsat and WorldView-2 scene the commonly used Normalized Difference Vegetation Index (NDVI), a spectral index based on the differences of the red and near infrared radiances [cf. (Carlson & Ripley, 1997; Nouri, Beecham, Anderson, & Nagler, 2013; Pettorelli et al., 2005; Tucker, 1979)]. The

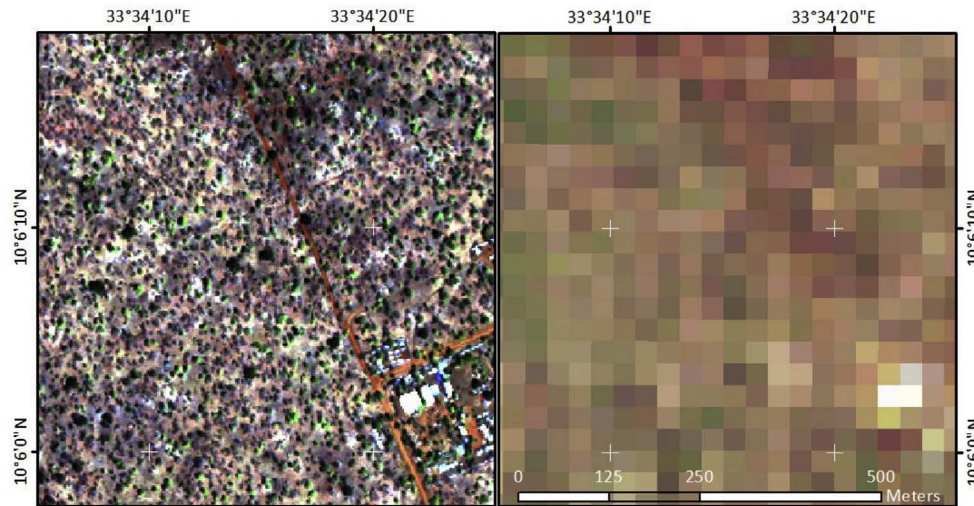


Fig. 2. Subsets of WorldView-2 (left) and Landsat 8 (right) images for the same area, illustrating the large difference in spatial resolution (2 × 2 m vs. 30 × 30 m).

NDVI was selected as it is a widely used and very robust indicator for vegetation and more specific a strong predictor variable for tree canopy cover (Karlson et al., 2015).

To integrate and combine information from the different datasets, we transferred all data given in a geographic coordinate system (e.g., WorldView-2 and in situ data) to the UTM projection which is used for the Landsat data. Afterwards we co-registered the data to ensure that the different spatial data sets are properly aligned to each other. Due to the significant temporal difference between the WorldView-2 data acquired at the beginning and at the end of the dry season, the vegetation cover exhibits differences in foliage and phenological stages. To account for these differences, we analysed the acquisitions from April and November/December separately and mosaicked individual WorldView-2 tiles according to their temporal cluster.

### 3.1.2. In situ data

Based on the pan-sharpened WorldView-2 images, 82 suitable field plots for ground truth measurements were identified considering the vegetation structure (i.e. focusing on homogeneous areas) and accessibility (cf. Appendix A.1 and A.2). The ground truth was acquired during a field campaign from 29 April to 8 May 2014 [cf. (Bloesch, 2014)]. Out of the 82 proposed field plots, 30 field plots were selected. The selection was determined by 2 factors: first, the field plots needed to have a certain distance to the refugee camps/settlement to avoid ongoing disturbances by tree cutting which complicate any calibration of the satellite data and second, the field plots needed to be accessible, both in terms of safety and general accessibility.

The field plots have been located using both, a handheld Garmin GPS (62S) and a Samsung Galaxy Tab3 with GPS showing the digital map sections with the corresponding sites. For each selected field plot, a homogenous area of an approximated minimum size of at least 0.25 ha within the plot has been selected for the survey and its centre has been recorded with its coordinates. Each plot centre was photographed in

each cardinal direction with a GPS camera (Panasonic Lumix DMC-TZ10) and additionally marked with the handheld GPS. In total, more than 300 GPS photographs have been obtained to aid the tree species identification and its assignment on the VHR satellite data.

For the detailed characterization of the vegetation within the selected field plots, a circular sample plot of 0.1 ha (radius of 17.85 m) has been surveyed including a detailed description of the vegetation type and dendrometric measurements. Examples for the respective vegetation types are visualized in Fig. 4, whereby riverine forests were determined as woodland within a 100 m wide belt to each side of watercourses.

Among other parameters, vegetation type and cover, and for all shrubs and trees, number per species, height, diameter at breast height, and actual foliage were recorded [cf. (Bloesch, 2014)]. The detailed classification scheme for the vegetation types and the number of visited field plots for each vegetation type is given in Table 2, whereby the respective thresholds of tree/shrub canopy cover were defined according to Bloesch (Bloesch, 2002). As can be seen from the table, for some of the vegetation types there are fewer samples than for others. This may have an impact on the classification results, but it should be noted that the vegetation types with the few sample plots also have a lower variability in coverage and species-specific characteristics.

In addition, vector data of the refugee camps, infrastructure, administrative borders and watercourses were available from UNITAR (United Nations Institute for Training and Research) and OpenStreetMap (<http://www.openstreetmap.org>).

### 3.2. Methods

To ensure a better comprehensibility of the developed method and of the different, partly sequential individual steps, the complete process flow of the procedure presented by us is schematically presented in Fig. 5.

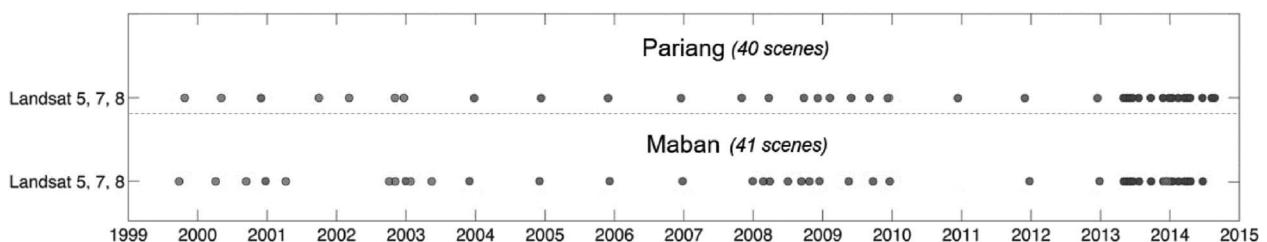


Fig. 3. Overview of the acquisition dates of the used 81 Landsat scenes for both counties.

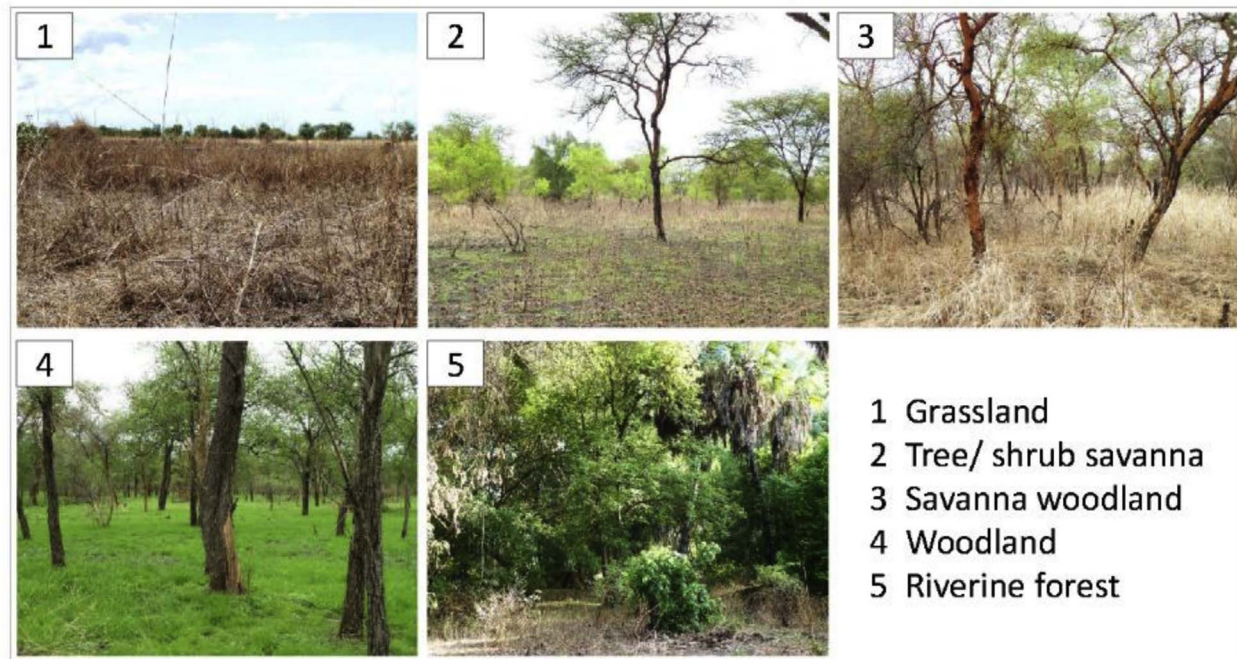


Fig. 4. Examples of assessed vegetation types.

**Table 2**  
Recorded vegetation types with respective canopy cover ranges.

Vegetation type	Canopy cover	Number of field plots
Grassland	≤ 2%	3
Tree/shrub savanna	2 - 30%	11
Savanna woodland	30 - 60%	8
Woodland	≥ 60%	3
Riverine forest	≥ 60%	5

3.2.1. Vegetation type classification

As in our study the vegetation types are defined by the canopy cover ranges (cf. Table 2), the approach to classify the different vegetation types is mainly based on the calculation of tree and shrub canopy cover. Due to differences in data availability (i.e. spatio-temporal coverage) and sensor characteristics (mainly in terms of spatial resolution) between the Landsat and WorldView-2 data, however, we applied different classification approaches.

For the WorldView-2 data, we firstly investigated for the field plots the relation between the in-situ data of tree and shrub canopy cover (cf. section 3.1.2) and the calculated NDVI values (cf. section 3.1.1) by

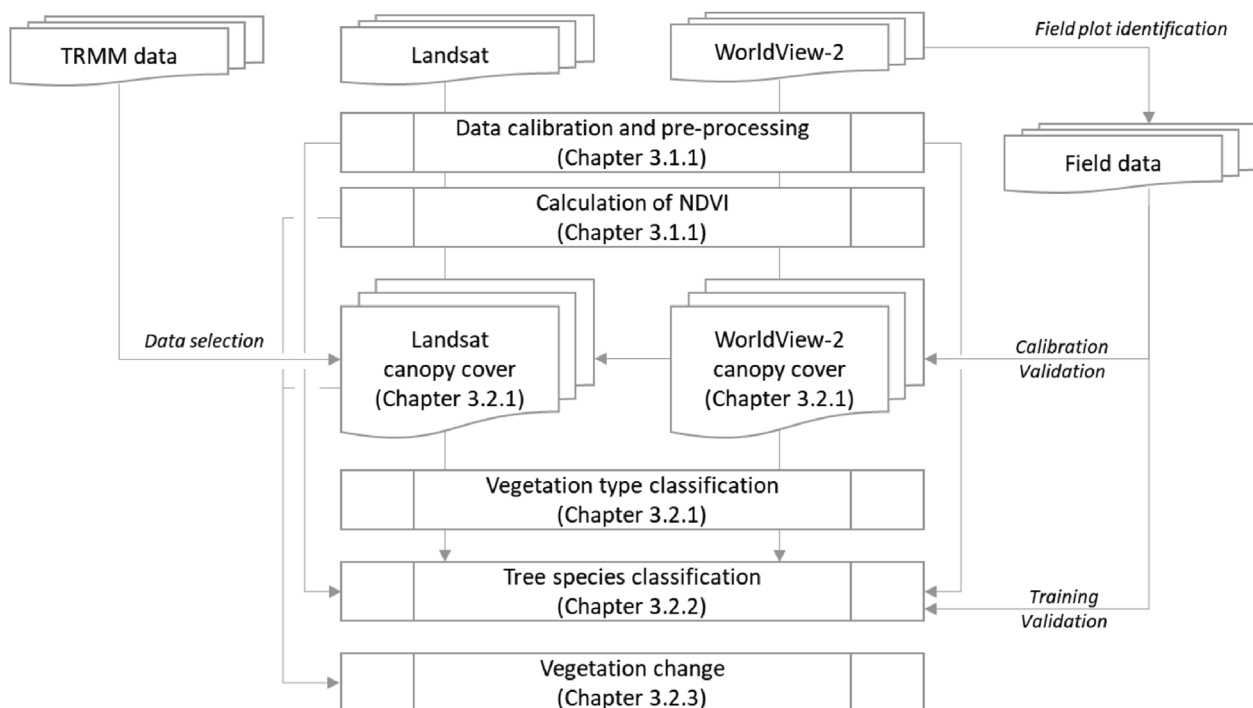


Fig. 5. Flowchart of the methods used in this study.

applying a regression analysis. To ensure comparable phenological stages of the vegetation, we only included WorldView-2 data from April (similar period as the field campaign) into the subsequent analysis. The comparison showed a good correlation coefficient of 0.68, meaning that WorldView-2 based NDVI values are highly correlated with in situ estimates of canopy cover. To estimate the optimal NDVI threshold for the derivation of the canopy cover, we quantified the root mean squared error between the different NDVI-based canopy cover estimates and the survey data. The lowest deviation between both datasets is given for a NDVI threshold of 0.37, which was subsequently used to classify each  $2 \times 2$  m pixel in all the WorldView-2 scenes as vegetation or non-vegetation. This initial classification also served as a vegetation mask for the tree species classification described in chapter 3.2.2. To meet the user requirements from the local natural resource management authorities, this  $2 \times 2$  m spatial resolution data set was downscaled to  $100 \times 100$  m (i.e. 1 pixel = 1 ha), integrating 2500 Boolean vegetation measurements per pixel. This pre-defined area of 1 ha is the standard spatial unit valid and used for the community forest management plan in South Sudan. Afterwards, for each 1 ha pixel the percentage amount of pixel classified as vegetation was calculated.

Non-photosynthetic vegetation, however, is not considered so far. We thus additionally classified the WorldView-2 scenes acquired during start of dry season (November/December) to identify areas where shrub/tree canopy cover is  $\geq 2\%$  (cf. Table 2) in November/December and  $\leq 2\%$  in April, representing seasonal non-photosynthetic vegetation. This classification approach was based on Support Vector Machine (SVM) classification (Cortes & Vapnik, 1995; Foody & Mathur, 2004) using ENVI® software. SVM is a supervised classification method derived from statistical learning theory that often yields good classification results from complex and noisy data (Foody & Mathur, 2004; Pal & Mather, 2005; Schneider, 2012). It separates the classes with a decision surface that maximizes the margin between the classes. The respective field plots with the ground truth measurements in Maban were used as training data for the SVM classifier.

Based on the classification results, we included the non-photosynthetic vegetation class in the foregoing derived NDVI based classification of vegetation. Finally, the tree and shrub coverage was classified according to the predefined canopy cover ranges (cf. Table 2).

Due to the lower spatial resolution of the Landsat data ( $30 \times 30$  m pixel size), each Landsat pixel contains generally a mixture of vegetation, soil and other surface materials. This heterogeneity makes a distinction between trees/shrubs and grasslands infeasible during the rainy season. However, as indicated by Bloesch (Bloesch, 2014), there is a limited time frame during 4–6 weeks after the last rainfall event ( $> 2$  mm), when grasslands turned already from a photosynthetic to a non-photosynthetic state while trees are remaining still photosynthetically active. Taking advantage of these phenological differences, we used TRMM (Tropical Rainfall Measuring Mission) satellite data [cf. (Huffman et al., 2007)] to detect the start of the dry season and thus the timeframe for useful Landsat acquisitions (cf. Fig. 6). The detection of the tree/shrub coverage using the Landsat data was thus

based on complementary expert knowledge about the vegetation characteristic and additional TRMM data indicating the onset of the dry season.

For the classification, we applied the same approach for determining the NDVI threshold as previously described for the WorldView-2 data. The direct comparison of the Landsat NDVI values with the in-situ estimates of canopy cover, however, yields to a very low correlation coefficient of 0.36, mainly caused by the large temporal variability of the pixel-based NDVI values (e.g., due to existing data gaps in Landsat caused by a high cloud cover). Thus, we established a relation between the Landsat NDVI data and the rescaled (to  $30 \times 30$  m) WorldView-2 vegetation classification, allowing the same method for an optimized NDVI threshold determination as for the WorldView-2 data (cf. Appendix A.3). As applied for the WorldView-2 data, we finally downscaled the calculated tree and shrub coverage to 1 ha pixel size and applied the classification scheme according to the Yangambi vegetation types (cf. Table 2).

### 3.2.2. Tree species classification

For the tree species classification, we tested different common supervised classification algorithms. In general, supervised classifications are based on representative samples for each classification class. These calibration samples or training data are used to identify the respective classes in the entire image based on their spectral signature. In case of the applied tree species classification (i.e. the classification of the four dominating tree species Red acacia, Dessert date tree, Silak, and Doum palm) the calibration data was based on the in-situ forest inventory data (cf. section 3.1.2.), whereby only half of the data was used to train the supervised classification algorithms and half of the data for the validation. For Maban county we supplemented the validation data based on the visual interpretation of tree species-specific spectral and structural characteristics. For example, Desert date tree typically occurs more isolated with an irregular tree crown shape and often dominant near settlements. Furthermore, we used additional information on vegetation types from the land-cover sites description [cf. (Bloesch, 2014)] to verify our visual interpretation results.

For the classification, we tested the performance of 3 supervised classification algorithms: i) SVM as a supervised classification method derived from statistical learning theory (Cortes & Vapnik, 1995; Pal & Mather, 2005), ii) Spectral Angle Mapper (SAM) as a physically-based spectral classification (Cho et al., 2010; Kruse et al., 1993), and iii) Maximum Likelihood (ML) as a method of selecting the set of values of the model parameters that maximizes the likelihood function (Defries & Townshend, 1994; Foody, Campbell, Trodd, & Wood, 1992). For both, the Landsat and the WorldView-2 data the multi-temporal information content was used to capture characteristic phenological vegetation conditions. In contrast to the Landsat classification, however, the training-dataset for the WorldView-2 data is composed of individual tree spectra, which only includes canopy cover pixels rather than broader regions as illustrated for the Landsat data. In addition, a vegetation mask (cf. section 3.2.1) was used to masked-out soils and other

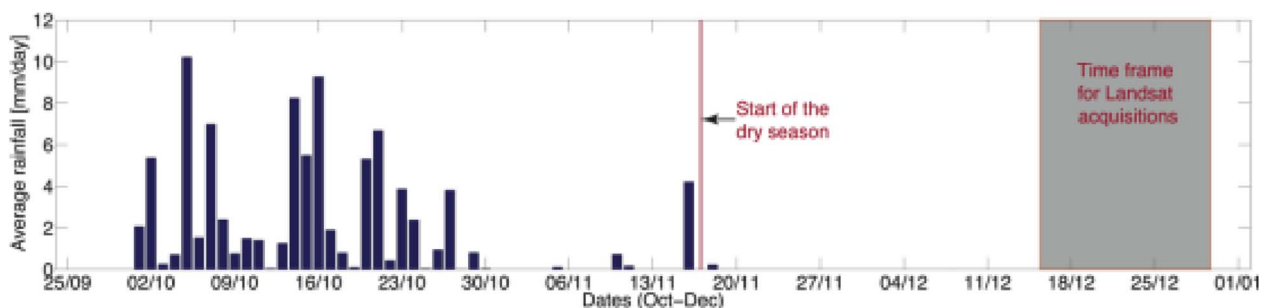


Fig. 6. Example of daily rainfall events in Maban during October to December as indicated by TRMM data. The last rainfall event ( $> 2$  mm) marks the end of the rainy season and sets the time frame for suitable Landsat acquisitions to distinguish between trees/shrubs and grasslands.

non-vegetated land cover from the classification. The resulting tree species classification was afterwards intersected with the vegetation types savanna woodland and woodland, as only for these vegetation types the number of trees (i.e. the tree canopy cover – cf. section 3.1.2) is sufficient large enough for a tree species classification based on the spectral characteristics of the canopies.

### 3.2.3. Vegetation change

To assess changes in the vegetation canopy cover that occurred after the refugees arrived in South Sudan, we used the multi-temporal Landsat data only. First, we detected canopy cover changes based on the NDVI values between the periods 2000 to 2010 (before the arrival of the refugees) and 2012 to 2013 (after the arrival of the refugees). This change analysis encompasses all kind of vegetation changes, including variations in grassland, tree and shrub canopy cover. To analyse changes in the amount of accessible wood resources, we assessed in a second step the changes in canopy cover only for savanna woodlands and woodlands. This analysis was based on the NDVI values at the onset of the dry seasons during the years 2000–2013, as at that time the grass layer is mostly photosynthetically inactive while mainly trees and shrubs are depicted by the NDVI.

The proposed method, however, is hampered by various challenges, such as annually varying vegetation characteristics (due to varying precipitation patterns), data gaps by cloud cover, and changing surface characteristics due to different fire histories. Our approach to overcome these challenges is based on incorporating data from multiple years, selecting comparable datasets from different years, and levelling data to account for annual variations. We therefore used multiple datasets, which were averaged over multiple years/seasons to compensate for data gaps such caused by cloud cover or severely burnt areas. For the assessment of changes in the wood resources, scenes that were obtained during a similar time of the year with a comparable scene-average NDVI were selected. To finally quantify changes in the surrounding of and within the refugee camps/settlement, we calculated the relative changes in NDVI and related those to changes in the canopy cover based on the NDVI-canopy cover relation (cf. chapter 3.2.1).

### 3.2.4. Validation

We validated the vegetation type and tree species classification with the in-situ measurements. All used accuracy metrics are based on the confusion matrix, which shows the accuracy of a classification result by comparing it with the in-situ measurements. The accuracy metrics derived include the overall accuracy (OA), producer's (PA) and user's accuracy (UA) (Liu, Frazier, & Kumar, 2007), as well as the quantity difference (QD) and the allocation difference (AD) (Pontius & Millones, 2011). QD is defined as 'the amount of difference between the reference map and a comparison map that is due to the less than perfect match in the proportion of the categories', whereas AD is defined as 'the amount of difference between the reference map and a comparison map that is due to less than the optimal match in the spatial allocation of the categories, given the proportions of the categories in the reference and comparison maps' (Pontius & Millones, 2011). Following Pontius & Santacruz (Pontius & Santacruz, 2014), AD is further separated into the two components exchange and shift. Exchange is the component of allocation difference that pairwise confusions cause, whereas shift is the component of allocation difference that nonpairwise confusions cause.

## 4. Results

### 4.1. Vegetation type classification

Fig. 7 shows as an example for Maban the calculated tree and shrub canopy cover for both the WorldView-2 and the Landsat data with a spatial resolution of 1 ha. The differences in the classified tree canopy cover and other limitations of the applied classification approach will be discussed in more detail in section 5.1.

Given the two different datasets and methodologies to derive tree and shrub canopy cover, we cross-compared both dataset and evaluated their performance by validating it with the in-situ data (cf. section 3.1.2). Although the Landsat estimates depict the general trend in tree and shrub canopy cover, the calculation based on WorldView-2 shows a slightly better agreement with the in-situ data (Fig. 8).

Because of the differences in canopy cover calculation (cf. Fig. 7), the consequent classification of vegetation types shows comparable patterns between Landsat and WorldView-2 data (Fig. 9). For example, it is clearly visible that particularly in the surrounding of the Kaya camp and along the Yabus river the Landsat-based classification show lower coverages of savanna woodland and woodland.

### 4.2. Tree species classification

The SVM classification shows for both, the Landsat and the WorldView-2 data, the best results compared to the SAM and ML classifiers. For Maban, the SVM classification based on the Landsat data resulted in an overall accuracy of 62.6%, whereas the SAM and ML classifiers resulted in overall accuracies of 56.7% and 59.1%, respectively. The corresponding confusion matrix of the SVM classification is based on the classified pixels and given in Table 3.

The corresponding quantity and allocation differences are shown in Fig. 10.

For Pariang we could not implement the same approach as the data set on vegetation sites was comparably small. Nevertheless, we used all available land cover and vegetation survey sites to create a training dataset that included seven regions for three tree species (Red Acacia, Desert date tree, Silak). The overall accuracy among these training datasets is very high but of low explanatory power. Nevertheless, it is supporting the argument that the classification algorithm can spectrally distinguish individual tree classes. Fig. 11 illustrates the results of the classification for both Pariang and Maban.

The respective proportions of area for each vegetation type and tree species class is given in Table 4.

The tree species classification based on the WorldView-2 data leads to comparable accuracies (Table 5/Fig. 12).

The results for the WorldView-2 data, however, need to be viewed with caution, as the statistical base of reference data was suitable only to a limited extent for an evaluation at individual tree level. Fig. 13 shows an example for the tree species classification based on the WorldView-2 data for Maban.

### 4.3. Vegetation change

The change of canopy cover is shown as relative change between the periods 2000 to 2010 (before the arrival of the refugees) and 2012 to 2013 (after the arrival of the refugees). Positive values indicate an increase in canopy cover, whereas negative values indicate a decrease in canopy cover. There are only small changes in the canopy cover in the decade prior to the arrival of the refugees whereas larger changes happen after the arrival of the refugees in 2011. Figs. 14 and 15 depicts changes in tree and shrub canopy cover in the time periods 2000–2010 to 2012–2013, shown as relative changes in NDVI values.

As described in chapter 3.2.1, we related the changes in NDVI to changes in canopy cover based on the NDVI-canopy cover relation to quantify changes in the surrounding of and within the refugee camps. In Table 6, the changes in canopy cover for savanna woodlands and woodlands as an estimate for changes in the amount of accessible wood resources are listed for the different refugee camps/settlement and within a buffer zone of 3 km around the camps/settlement. The changes in canopy cover generally decrease with increasing distance from the refugee camps/settlement.

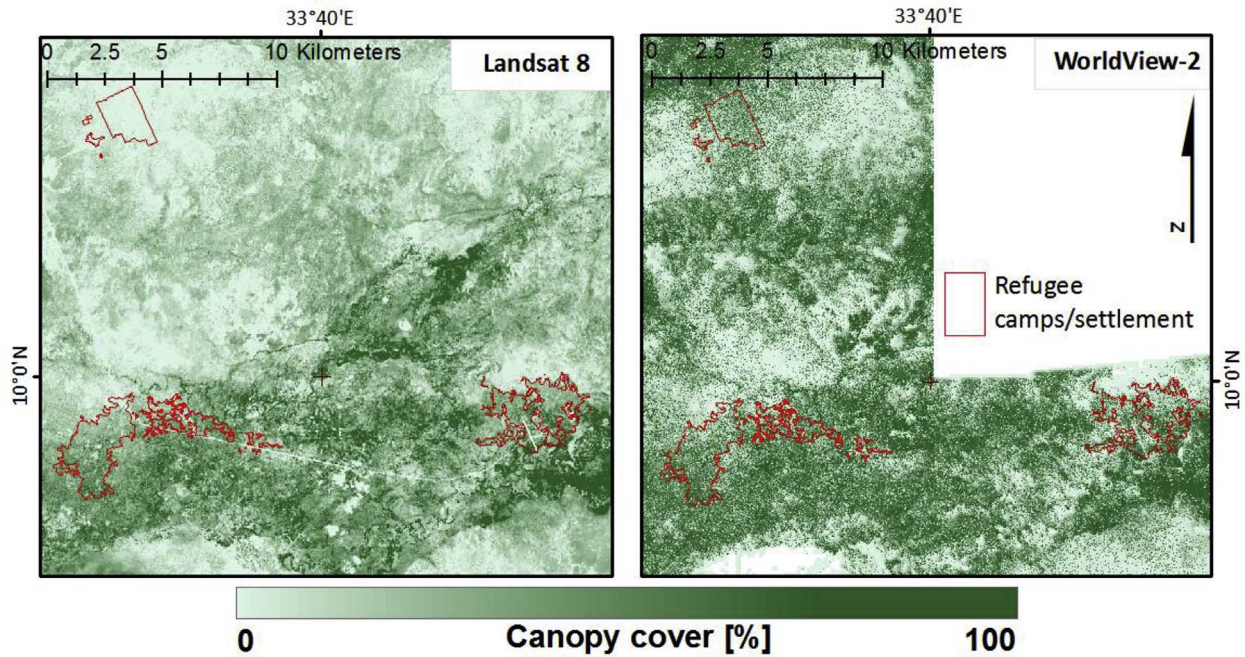


Fig. 7. Canopy cover for a subset of Maban based on Landsat-8 (left) and WorldView-2 (right).

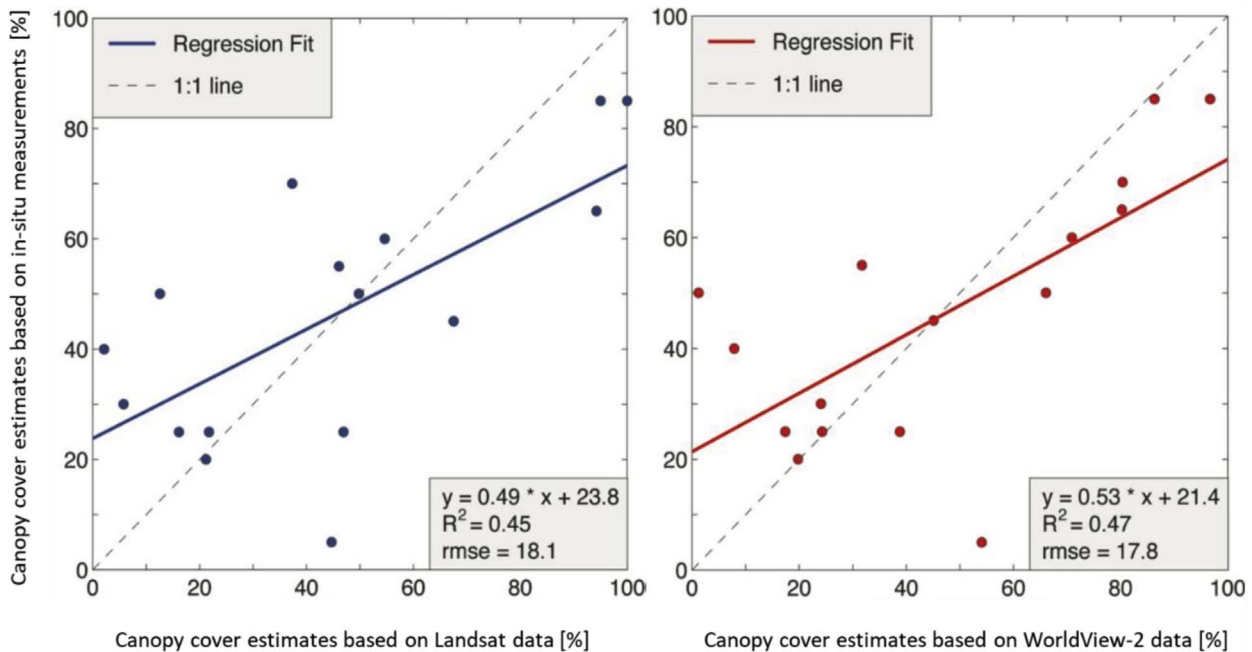


Fig. 8. Regression analysis between Landsat and WorldView-2 derived canopy cover estimates and canopy cover estimates based on the field survey.

## 5. Discussion

### 5.1. Vegetation type classification

The results of the vegetation type classification are comparable with the findings by Zeidler et al. (Zeidler et al., 2012), Boggs (Boggs, 2010), and Adjorlolo and Mutanga (2013). Even if the WorldView-2 data could provide more detailed maps of the vegetation types, the difference to the Landsat based classification is negligible and thus would not justify the operational necessity for the use of commercial VHR EO data [cf. (Heiskanen et al., 2017)]. It is noticeable, however, that the Landsat-based calculation of canopy cover shows in comparison to the

WorldView-2 based classification lower coverages of savanna woodland and woodland, particularly in the surrounding of the Kaya camp and along the Yabus river. Part of the differences can be explained by the widespread occurrence of Silak trees, which could interfere the performance of the SVM classification algorithm due to their specific phenology and the very loose foliage, as well as in the wetland areas along major rivers.

The only marginally better results of the WorldView-2 based classification could be caused by the pixel-based approaches used by us. As it was shown in several previous studies, the advantage of VHR EO mainly becomes apparent when they are used on the object level (Blaschke et al., 2014; Chen, Hay, Carvalho, & Wulder, 2012; Hussain,

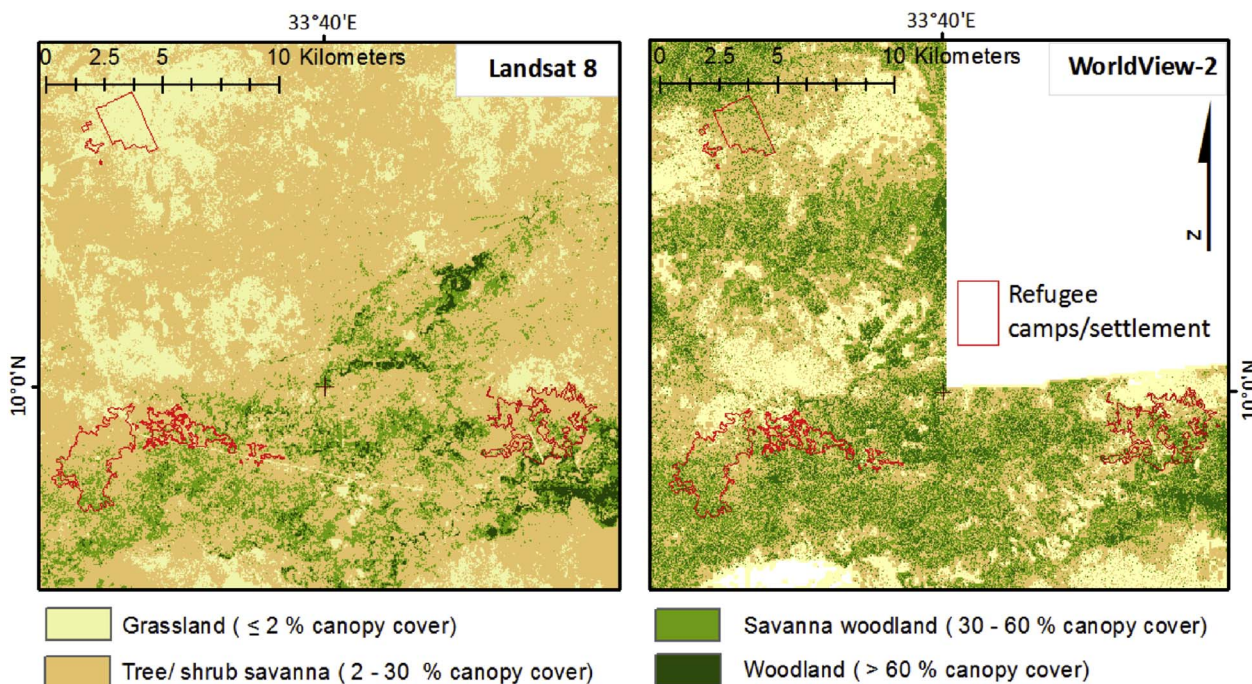


Fig. 9. Vegetation type classification for a subset of Maban based on Landsat-8 (left) and WorldView-2 (right) for the year 2013.

Table 3

Confusion matrix of the tree species classification for Maban (based on Landsat data) with user's (UA), producer's (PA), and overall accuracy (OA).

Classification	Reference				UA (%)
	Red Acacia	Silak	Desert date tree	Doum palm	
Red Acacia	1849	230	173	541	66.2%
Silak	3109	1511	2	14	32.6%
Desert date tree	1902	95	7405	0	78.8%
Doum palm	358	0	0	7	1.9%
PA (%)	25.6%	82.3%	97.7%	1.2%	
	OA = 62.6%				

Chen, Cheng, Wei, & Stanley, 2013). Nevertheless, also object based image analysis has challenges, such as selecting optimal segmentation scales, and most of the studies focus on urban or agricultural

environments, in which clear, and more easily distinguishable shapes are frequently occur (Addink, De Jong, & Pebesma, 2007; Liu & Xia, 2010). The advantage of the proposed approach, however, is the scalability and robustness of the method, which allows the automatic mapping of vegetation types on a regional level.

Nevertheless, there are limitations of the approach which need to be considered. Deviations between the Landsat and WorldView-2 vegetation type classifications could be caused by different vegetation conditions between the years, slight misjudgements of canopy cover estimates in the field, uncertainties in the geolocation of the satellite data or BRDF (Bidirectional Reflectance Distribution Function) effects due to off-nadir satellite viewing angles. Furthermore, it should be noted that extended areas in southern Pariang along the Bahr el Ghazal River are wetlands with lush grasslands throughout the year. Like these wetlands, topographic depressions occur in both counties, which hold water for extended periods into the dry season. These grasslands are photosynthetically active during the first months of the dry-season.

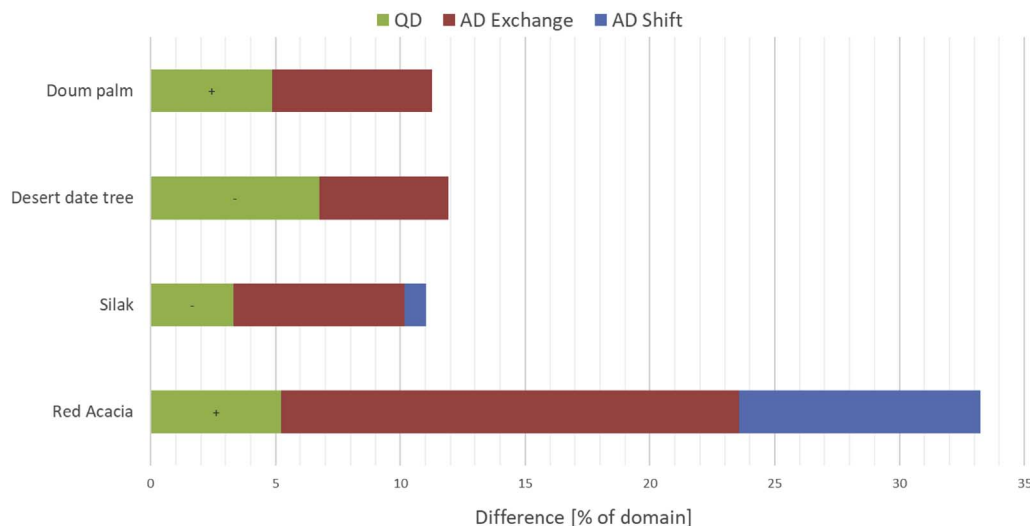


Fig. 10. Quantity (QD) and allocation (AD) disagreements of the tree species classification for Maban (based on Landsat data).

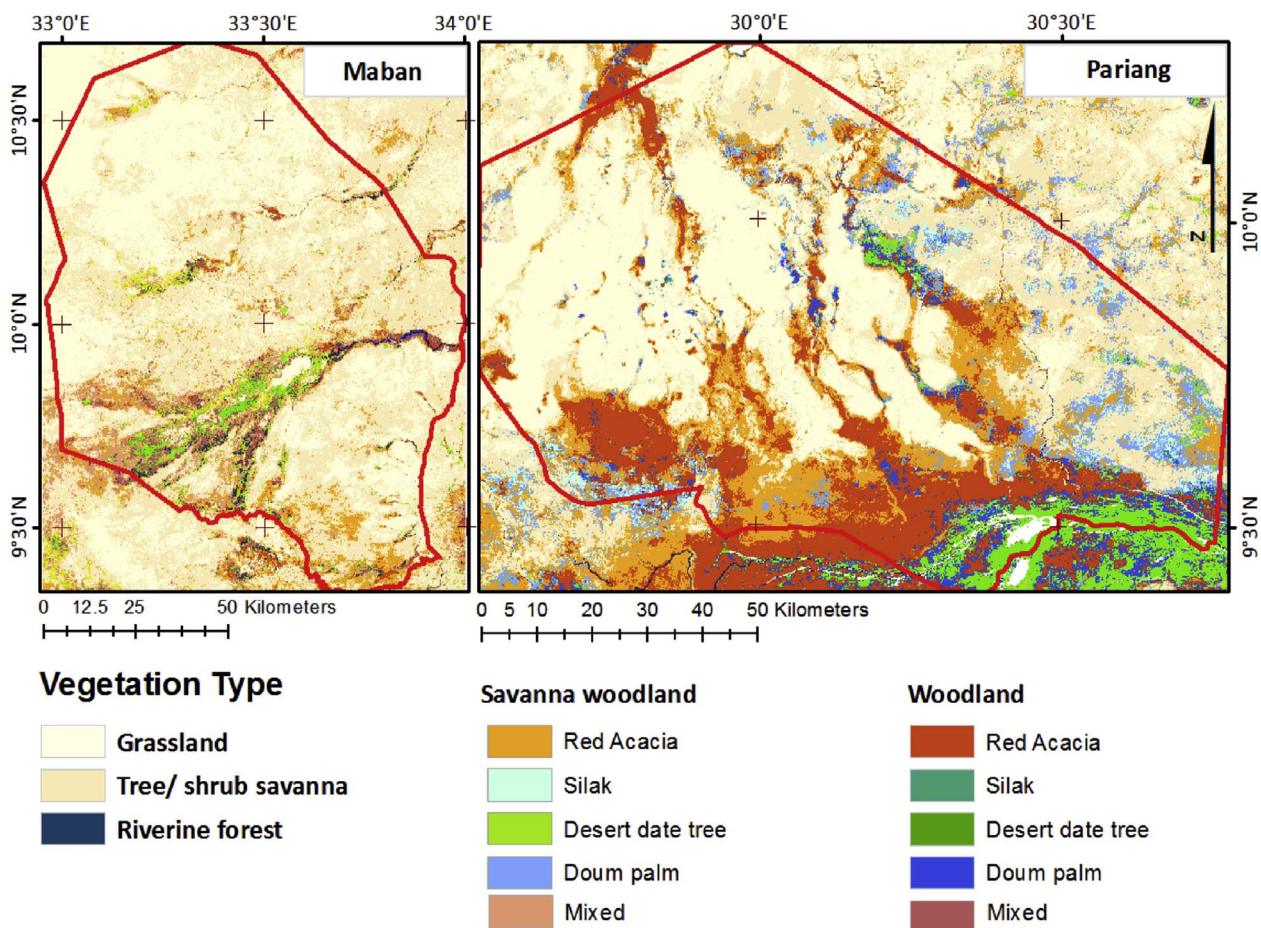


Fig. 11. Classification of vegetation types and tree species (for vegetation types “savanna woodlands” and “woodlands”) in Pariang and Maban using Landsat data.

**Table 4**  
Area proportions for the respective vegetation type and tree species classes.

Vegetation type	Tree species	Maban		Pariang	
		Area [km <sup>2</sup> ]	Area [%]	Area [km <sup>2</sup> ]	Area [%]
Water		0.0	0.00	50.0	0.56
Grassland		4382.5	36.95	2890.5	32.38
Tree/shrub savanna		5187.6	43.74	2159.2	24.19
Savanna woodland	<i>Red Acacia</i>	563.5	4.75	1334.4	14.95
	<i>Desert date tree</i>	213.9	1.80	44.8	0.50
	<i>Silak</i>	155.1	1.31	170.9	1.91
	<i>Doum palm</i>	1.4	0.01		
	<i>Mixed</i>	706.0	5.95	494.6	5.54
Woodland	<i>Red Acacia</i>	90.8	0.77	1240.0	13.89
	<i>Desert date tree</i>	144.0	1.21	254.7	2.85
	<i>Silak</i>	91.4	0.77	12.4	0.14
	<i>Doum palm</i>	5.3	0.05		
Riverine Forest	<i>Mixed</i>	294.4	2.48	264.3	2.96
		25.0	0.21	9.7	0.11
Total area		11861.1	100	8925.6	100

Therefore, these grasslands are characterized by high NDVI values even after the onset of the dry season. Consequently, with the proposed approach the vegetation type in these regions is partly misclassified as woodland, which should be considered while interpreting the resulting maps.

Moreover, the onset of the dry-season is also characterized by pronounced fire activity as the vegetation dries up and allows for fire propagation. Burned areas exhibit a significantly reduced spectral

**Table 5**  
Confusion matrix of the WorldView-based SVM classification (based on WorldView-2 data) of tree species for Maban.

Classification	Reference				
	Red Acacia	Silak	Desert date tree	Doum palm	UA (%)
Red Acacia	431	79	48	263	52.5%
Silak	342	33	6	11	8.4%
Desert date tree	187	11	978	2	83.0%
Doum palm	2	8	3	21	61.8%
PA (%)	44.8%	25.2%	94.5%	7.1%	
					OA = 60.3%

reflectance in the visible and near infrared wavelength regions, which leads to a NDVI decrease that correlates to proportion of soil-vegetation mixture per pixel. Therefore, canopy cover in such burnt areas could be captured in a lower degree as it is. Our approach to use Landsat data from several years, however, may attenuate these effects as, among other things, the specific vegetation types show in general very high recovery rates (Gatebe, Ichoku, Poudyal, Román, & Wilcox, 2014; Gomes et al., 2014; Lambin, Goyvaerts, & Petit, 2003).

### 5.2. Tree species classification

The results of the tree species classification in Tables 3 and 4 shows, that the class specific accuracies vary widely. While the classification of Red Acacia and Desert date tree shows satisfactory classification results in terms of the user's accuracies, the Doum palm cannot be reliably mapped. For both, the Landsat and WorldView classification

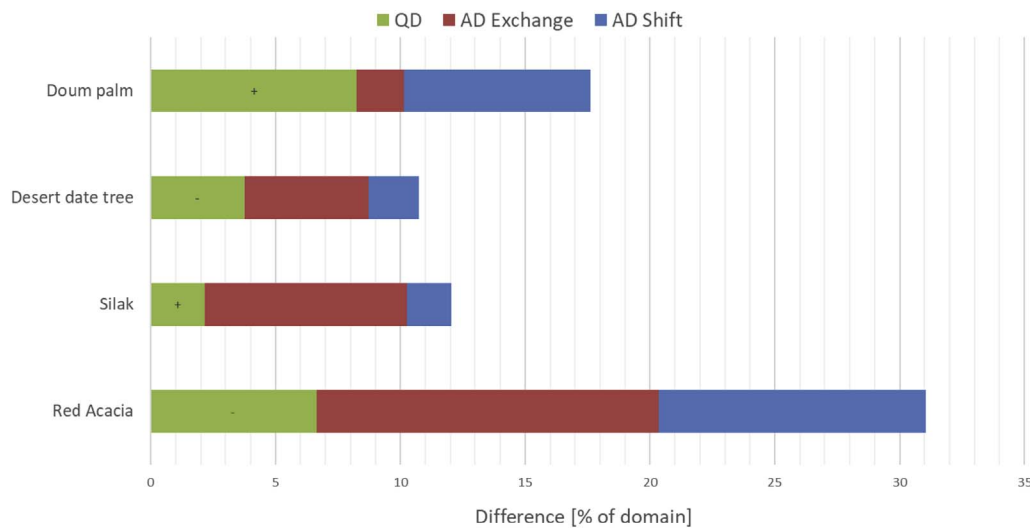


Fig. 12. Quantity (QD) and allocation (AD) disagreements of the tree species classification for Maban (based on WorldView-2 data).

approaches, the major part of class uncertainty is due to rather high allocation disagreements. This counts particularly for the classification of Red Acacia. The main quantity disagreements, however, arise for Desert date tree (for the Landsat classification) and for Doum palm and Red acacia (for the WorldView classification). Moreover, even if most of the reference Silak trees were correctly identified, there is a high overlap with the Red Acacia classification, i.e. the commission error for this class is rather large. These differences could be mainly caused by the occurrence pattern of the specific tree species. Desert date tree, for example, occurs in larger homogeneous patches, whereas the Doum palm often occurs as single tree or in smaller groups of 3–4 individuals. Particularly using the Landsat data, individual trees or smaller groupings of trees are difficult to identify due to the coarser spatial resolution. In contrast, the higher spatial resolution of the WorldView-2 data leads to problems caused by the heterogeneity within the canopy cover. Due to its high resolution, differences in illuminated and shaded parts under the tree crown can result in different spectral classes, as the shaded parts are spectrally more similar among each other (cf. section 5.1). Previous research, however, has shown that data from WorldView-2 seems to be a suitable way for the classification of tree species, particularly if object based classification approaches were applied (Colgan, Baldeck, Féret, & Asner, 2012; Immitzer et al., 2012; Pu et al., 2015).

The results of the tree species classification presented in this study could be improved accordingly, if object-based classification approaches or a combination of pixel and object-based analysis would be applied.

Nevertheless, previous studies about tree species classification for semi-arid savanna ecosystems were mainly carried out on local scales and based on airborne EO data, e.g. derived with airborne laser scanning or imaging spectroscopy [cf. (Cho et al., 2012; Colgan et al., 2012; Naidoo, Cho, Mathieu, & Asner, 2012)]. To the best of our knowledge, tree species classifications based on Landsat data were not applied so far in these African semi-arid savanna ecosystems and/or not on a county level. We therefore cannot directly compare our results to existing studies, but feedbacks from the forest service and UNHCR and its implementing partners show, that the vegetation map including information of the distribution of the most important tree species is very useful for defining management actions, despite the different classification accuracies of the specific tree species. The classification approach itself, nevertheless, includes several uncertainties, which should be considered while interpreting the results.

First, as we labelled our calibration/training dataset according to the dominant tree species, it incorporates other tree species present at varying degrees (0–50%) in the vegetation survey sites. This can lead to

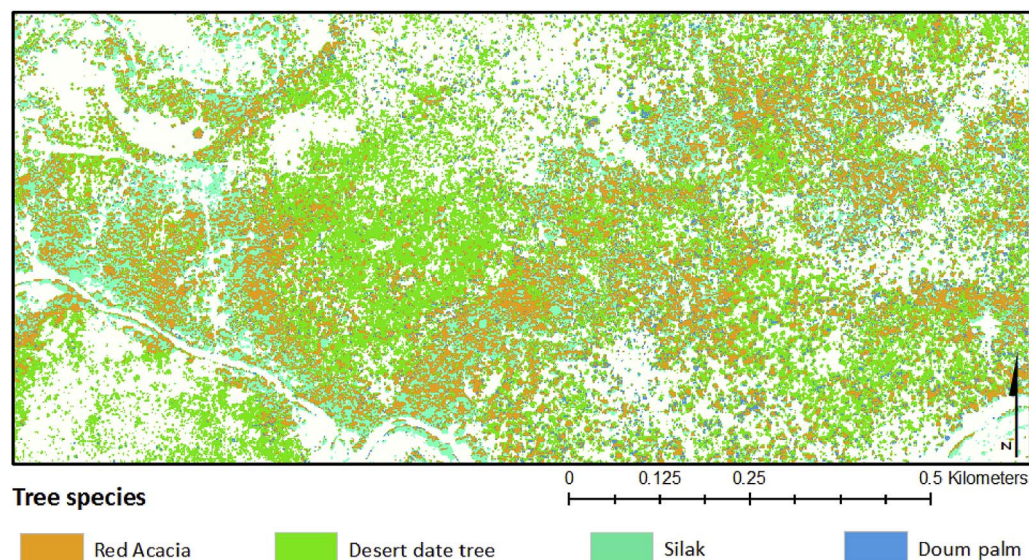


Fig. 13. Detail of the classification of tree species for savanna woodlands and woodlands in Maban county using the multi-temporal WorldView-2 data.

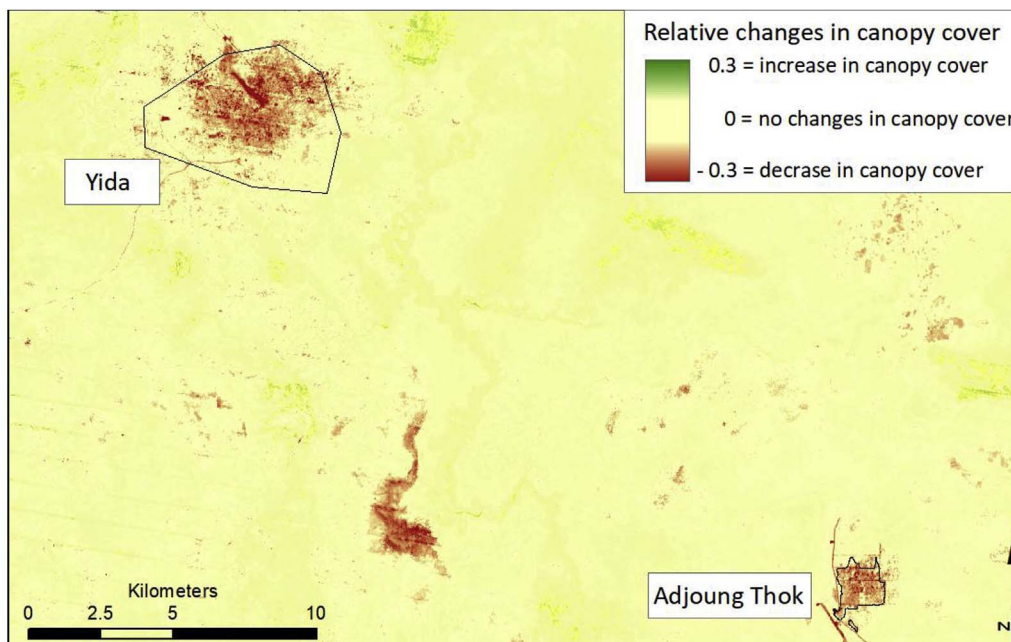


Fig. 14. Relative changes in tree and shrub canopy cover (shown as relative NDVI changes) for the area with refugee camps/settlement in Pariang (2000–2010 to 2012–2013).

an underrepresentation of tree species, which are more dispersed and do not occur in homogeneous groups. Second, we extended the spatial extent of the survey sites based on visual interpretation of the available satellite imagery, which introduced a growing uncertainty of the tree species present. Third, the survey sites are labelled according to their dominant tree species, irrespective of their canopy cover. As a result, varying degrees of mixed pixel (i.e. pixels including varying fractions of vegetation and soil) influence the spectral tree-species fingerprint. Fourth, randomly missing data due to cloud cover in some Landsat scenes introduces a bias in the classification, as certain seasonal information is missing. Fifth, burnt areas alter the spectral response of soils as they significantly decrease their spectral reflectance. Therefore, fire in areas with a low canopy cover (e.g. tree/shrub savannas) and

Table 6

Changes in canopy cover for savanna woodlands and woodlands within the area of the refugee camps/settlements and for a 3 km buffer zone around the camps/settlement (indicated in brackets).

Refugee camps/settlements	Relative changes in canopy cover for savanna woodlands and woodlands [%]
Adjoung Thok (Pariang)	-50.60 (-26.94)
Yida (Pariang)	-25.09 (-5.74)
Batil/Gendrasa (Maban)	-9.89 (-11.67)
Doro (Maban)	-3.01 (+0.32)
Kaya (Maban)	-19.36 (-15.82)

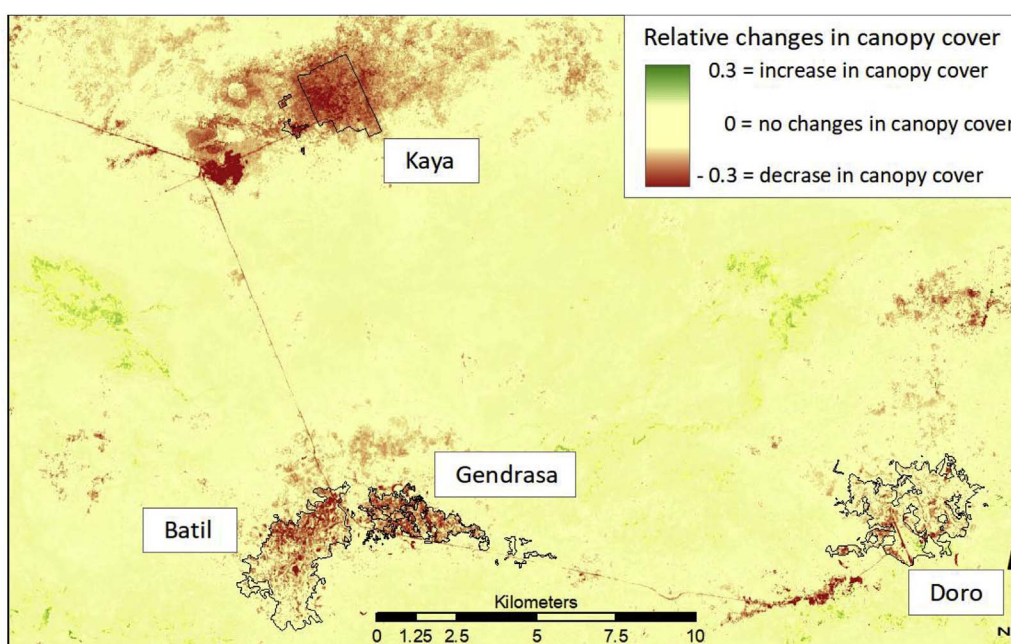


Fig. 15. Relative changes in tree and shrub canopy cover (shown as relative NDVI changes) for the area with refugee camps in Maban (2000–2010 to 2012–2013).

high proportion of mixed pixel will have a more profound impact on the spectral reflectance as compared to high canopy cover areas (e.g. woodlands) and can lead to misclassifications.

Regarding community forestry, the mapping of the woody formations of the savanna landscape in the Sudanese refugee-hosting areas of northern South Sudan provides a reliable basis for the estimation of the spatial availability of wood resources for the refugees and the host communities. The classification of vegetation units will enable a stratified sampling of the forest inventory [cf. (Bloesch, 2014)]. Moreover, the distinction of the four largely dominating tree species of great socio-economic importance (Red acacia, Dessert date tree, Silak, Doum palm) will highly increase the practical utility of the map. An accurate estimation of the wood resources (growing stock) and their productivity on the one hand, and the definition of their consumption on the other hand, will serve as a basis for a sustainable community forest management plan, including both, the host communities and the refugees. Thereby, our initiative will contribute to a conflict-sensitive management of the natural resource in the Sudanese refugee-hosting areas in South Sudan.

### 5.3. Vegetation change

The analysis of vegetation changes indicates a decrease of vegetation cover in the areas within as well as in the surroundings of the refugee camps/settlements. In comparison to vegetation change studies from other camps/settlements [e.g. (Gorsevski et al., 2013)], we received much higher values, i.e. a larger decrease in the vegetation cover. The decrease of vegetation in our study is mainly caused by deforestation (tree felling for shelter building material and fuelwood), animal grazing, and increased surface exposure by roads and shelters. The changes in woodland, however, are in general less pronounced in the refugee camp areas. This might be due to the low woodland canopy cover in the first place in some of the camps/settlement and that some tree species, for example the Desert date tree, are spared from tree cutting for cultural reasons (Bloesch et al., 2013). The assessment of the vegetation change will serve as valuable baseline data for planning purposes in general, and for monitoring ecosystem dynamics within and around the refugee camps/settlement.

### 5.4. Replication potential of the methods

Our approach of assessing vegetation changes within and around refugee camps/settlements and the mapping of woody formations at large scale considering the dominating tree species is of great practical value. There is an urgent need for more reliable data (baseline) on forest resources in large humanitarian operations. Therefore, there is a high replication potential of our methods for planning purposes of humanitarian actors in large camp settings for supporting the sustainable use of wood resources jointly by the host and displaced communities. Moreover, the same methods can be applied elsewhere by the national and local forest service to improve their mapping/inventory and monitoring of forests. However, an actual transferability of the methodology in practice is and remains very demanding, since the method is based on a lot of samples and in-situ measurements, which is particularly an issue in areas where the security situation is considerably more critical.

## 6. Conclusions

In this study, we show the potential of EO for humanitarian action. We propose a method to classify the main vegetation types and woody formations in northern South Sudan using multi-scale EO data as well as their changes over time to estimate the impact of the Sudanese refugee camps/settlement on the local ecosystems. We developed sophisticated methodologies combining remote sensing and in-situ data, exploiting sensor synergies (i.e. Landsat with WorldView-2) and building upon

local expert knowledge. We generated detailed vegetation type and tree species maps for the Counties of Pariang and Maban in South Sudan and quantified changes in the vegetation with focus on refugee camps/settlements. The resulting vegetation maps can serve as a basis to estimate the total amount of accessible wood resources, identify potential harvest areas, and support the definition of a sustainable use of wood for construction and cooking purposes for the refugee and host communities based on a community forest management. This knowledge of the available resources could lead to an easing of the situation between refugees and the local population and could enable a sustainable and more consensual use of resources. However, the very tight security situation in South Sudan related to the ongoing civil war prevented until now the joint elaboration of the community forest management plan with all key stakeholders.

Some recommendations to optimize the workflow for potential future projects on forest mapping and monitoring in South Sudan and elsewhere include the following points: Multi-annual, EO acquisitions at the beginning of the dry season before and after the refugee influx should be used to detect vegetation changes within and around refugee camps. Multiple (20–30) training and validation sites (accurately located by differential GPS) should be surveyed at the same seasonal time (or same time) as the satellite imagery acquisitions. Multi-seasonal VHR satellite imagery (such as from WorldView) of seamless cloud-free acquisitions at beginning and end of the dry season provides best means to spectrally distinguish between different tree species. As an alternative to the Landsat data, the free available, multispectral Sentinel-2 data with a  $10 \times 10$  m spatial resolution and a high revisit time of 5 days may provide better means to spectrally distinguish between shrub/tree savannas and grasslands on the County to State level.

## Acknowledgements

This study was supported by SDC (Swiss Agency for Development and Cooperation) and the Swiss National Point of Contact for Satellite Images (NPOC). We are very grateful to UNHCR for supporting and facilitating the study. The WorldView-2 data were kindly provided by UNITAR's (United Nations Institute for Training and Research) operational satellite applications programme UNOSAT.

## Appendix A. Supplementary data

Supplementary data related to this article can be found at <http://dx.doi.org/10.1016/j.apgeog.2018.01.013>.

## References

- Abdelsalam, A. A. (2014). *Charcoal from savanna woodlands in a REDD strategy: Case of Sudan*. Climate Change and Forest Ecosystems.
- Addink, E. A., De Jong, S. M., & Pebesma, E. J. (2007). The importance of scale in object-based mapping of vegetation parameters with hyperspectral imagery. *Photogrammetric Engineering & Remote Sensing*, 73(8), 905–912.
- Adjorlolo, C., & Mutanga, O. (2013). Integrating remote sensing and geostatistics to estimate woody vegetation in an African savanna. (2013). *Journal of Spatial Science*, 58(2), 305–322.
- Alam, S. A., & Starr, M. (2009). Deforestation and greenhouse gas emissions associated with fuelwood consumption of the brick making industry in Sudan. *The Science of the Total Environment*, 407(2), 847–852.
- Asner, G. P., & Heidebrecht, K. B. (2002). Spectral unmixing of vegetation, soil and dry carbon cover in arid regions: Comparing multispectral and hyperspectral observations. *International Journal of Remote Sensing*, 23(19), 3939–3958.
- Banskota, A., Kayastha, N., Falkowski, M. J., Wulder, M. A., Froese, R. E., & White, J. C. (2014). Forest monitoring using landsat time series data: A review. *Canadian Journal of Remote Sensing*, 40(5), 362–384.
- Blaschke, T., Hay, G. J., Kelly, M., Lang, S., Hofmann, P., Addink, E., et al. (2014). Geographic object-based image analysis - towards a new paradigm. *ISPRS Journal of Photogrammetry and Remote Sensing*, 87, 180–191.
- Bloesch, U. (2002). *The dynamics of thicket clumps in the Kagera savanna landscape, East Africa* PhD thesis (No. 14386). Shaker, Aachen: Swiss Federal Institute of Technology Zurich (ETH).
- Bloesch, U. (2014). *Forest mapping and pre-inventory of the Sudanese refugee hosting areas in Maban and Pariang counties, South Sudan (24 April – 12 May 2014)* Mission report part

- A/B. Berne: SDC/UNHCR. www.adonsonia-consulting.ch, Accessed date: 20 September 2016.
- Bloesch, U., Schneider, A., & Lino, C. J. T. (2013). Towards an environmental strategy for Sudanese refugee hosting areas in Upper Nile and Unity States, South Sudan. *Environmental inception mission 4–22 June 2013* www.adonsonia-consulting.ch, Accessed date: 20 September 2016.
- Boggs, G. S. (2010). Assessment of SPOT 5 and QuickBird remotely sensed imagery for mapping tree cover in savannas. *International Journal of Applied Earth Observation and Geoinformation*, 12(4), 217–224.
- Brandt, M., Tappan, G., Diouf, A. A., Beye, G., Mbow, C., & Fensholt, R. (2017). Woody vegetation die off and regeneration in response to rainfall variability in the west african sahel. *Remote Sensing*, 9(1), 39.
- C.S.A. (Conseil scientifique pour l'Afrique au sud du Sahara) (1956). *Phytogéographie-phytogeography. Réunion de spécialistes du C.S.A. en matière de phytogéographie. Yangambi (28 July - 8 August), London, Publ. Bureau C.C.T.A., no. 22.*
- Carlson, T. N., & Ripley, D. A. (1997). On the relation between NDVI, fractional vegetation cover, and leaf area index. *Remote Sensing of Environment*, 62(3), 241–252.
- Chander, G., Markham, B. L., & Helder, D. L. (2009). Summary of current radiometric calibration coefficients for Landsat MSS, TM, ETM+, and EO-1 ALI sensors. *Remote Sensing of Environment*, 113(5), 893–903.
- Chen, H., Guo, J., Zhang, Z., & Xu, C.-Y. (2013). Prediction of temperature and precipitation in Sudan and South Sudan by using LARS-WG in future. *Theoretical and Applied Climatology*, 113(3–4), 363–375.
- Chen, G., Hay, G. J., Carvalho, L. M. T., & Wulder, M. A. (2012). Object-based change detection. *International Journal of Remote Sensing*, 33(14), 4434–4457.
- Chen, J., Zhu, X., Vogelmann, J. E., Gao, F., & Jin, S. (2011). A simple and effective method for filling gaps in Landsat ETM+ SLC-off images. *Remote Sensing of Environment*, 115(4), 1053–1064.
- Cho, M. A., Debba, P., Mathieu, R., Naidoo, L., Van Aardt, J., & Asner, G. P. (2010). Improving discrimination of savanna tree species through a multiple-endmember spectral angle mapper approach: Canopy-level analysis. *IEEE Transactions on Geoscience and Remote Sensing*, 48(11), 5559438 4133–4142.
- Cho, M. A., Mathieu, R., Asner, G. P., Naidoo, L., van Aardt, J., Ramoelo, A., et al. (2012). Mapping tree species composition in South African savannas using an integrated airborne spectral and LiDAR system. *Remote Sensing of Environment*, 125, 214–226.
- Cissé, S., Eymard, L., Otlé, C., Ndioune, J. A., Gaye, A. T., & Pinsard, F. (2016). Rainfall intra-seasonal variability and vegetation growth in the Ferlo basin (Senegal). *Remote Sensing*, 8(1), 66.
- Climate-data (2017). *Climate South Sudan*. https://de.climate-data.org/region/1596/, Accessed date: 20 February 2017.
- Colgan, M. S., Baldeck, C. A., Féret, J. B., & Asner, G. P. (2012). Mapping savanna tree species at ecosystem scales using support vector machine classification and BRDF correction on airborne hyperspectral and LiDAR data. *Remote Sensing*, 4(11), 3462–3480.
- Cortes, C., & Vapnik, V. (1995). Support-vector networks. *Machine Learning*, 20(3), 273–297.
- Crespi, M., & de Vendictis, L. (2009). A procedure for high resolution satellite imagery quality assessment. *Sensors*, 9(5), 3289–3313.
- Defries, R. S., & Townshend, J. R. (1994). NDVI-derived land cover classifications at a global scale. *International Journal of Remote Sensing*, 15(17), 3567–3586.
- Foley, J. A., Ramankutty, N., Brauman, K. A., Cassidy, E. S., Gerber, J. S., Johnston, M., et al. (2011). Solutions for a cultivated planet. *Nature*, 478(7369), 337–342.
- Foody, G. M. (2010). Assessing the accuracy of land cover change with imperfect ground reference data. *Remote Sensing of Environment*, 114(10), 2271–2285.
- Foody, G. M., Campbell, N. A., Trodd, N. M., & Wood, T. F. (1992). Derivation and applications of probabilistic measures of class membership from the maximum-likelihood classification. *Photogrammetric Engineering & Remote Sensing*, 58(9), 1335–1341.
- Foody, G. M., & Mathur, A. (2004). A relative evaluation of multiclass image classification by support vector machines. *IEEE Transactions on Geoscience and Remote Sensing*, 42(6), 1335–1343.
- Gara, T. W., Murwira, A., Ndaimani, H., Chivhenge, E., & Hatendi, C. M. (2015). Indigenous forest wood volume estimation in a dry savanna, Zimbabwe: Exploring the performance of high-and-medium spatial resolution multispectral sensors. *Transactions of the Royal Society of South Africa*, 70(3), 285–293.
- Gatebe, C. K., Ichoku, C. M., Poudyal, R., Román, M. O., & Wilcox, E. (2014). Surface albedo darkening from wildfires in northern sub-Saharan Africa. *Environmental Research Letters*, 9(6), 065003.
- Gomes, L., Maracahipes, L., Marimon, B. S., Reis, S. M., Elias, F., Maracahipes-Santos, L., et al. (2014). Post-fire recovery of savanna vegetation from rocky outcrops. *Flora: Morphology, Distribution, Functional Ecology of Plants*, 209(3–4), 201–208.
- Gonzalez, P., Tucker, C. J., & Sy, H. (2012). Tree density and species decline in the African Sahel attributable to climate. *Journal of Arid Environments*, 78, 55–64.
- Gorsevski, V., Geores, M., & Kasischke, E. (2013). Human dimensions of land use and land cover change related to civil unrest in the Imatong Mountains of South Sudan. *Applied Geography*, 38(1), 64–75.
- Gorsevski, V., Kasischke, E., Dempewolf, J., Loboda, T., & Grossmann, F. (2012). Analysis of the Impacts of armed conflict on the Eastern Afromontane forest region on the South Sudan - Uganda border using multitemporal Landsat imagery. *Remote Sensing of Environment*, 118, 10–20.
- Haara, A., & Leskinen, P. (2009). The assessment of the uncertainty of updated stand-level inventory data. *Silva Fennica*, 43(1), 87–112.
- Hagenlocher, M., Lang, S., & Tiede, D. (2012). Integrated assessment of the environmental impact of an IDP camp in Sudan based on very high resolution multi-temporal satellite imagery. *Remote Sensing of Environment*, 126, 27–38.
- Hahn-Hadjali, K., & Schmid, S. (1999). Analysis of savanna communities in the Soudanian zone of Burkina Faso (Western Africa) with multitemporal SPOT satellite data [Untersuchungen von Savannengesellschaften der Sudanzone Burkina Fasos (Westafrika) mit multitemporalen SPOT-Satellitendaten]. *Die Erde*, 130(1), 1–16.
- Heiskanen, J., Liu, J., Valbuena, R., Aynekulu, E., Packalen, P., & Pellikka, P. (2017). Remote sensing approach for spatial planning of land management interventions in West African savannas. *Journal of Arid Environments*, 140, 29–41.
- Herrmann, S. M., & Tappan, G. G. (2013). Vegetation impoverishment despite greening: A case study from central Senegal. *Journal of Arid Environments*, 90, 55–66.
- Horion, S., Fensholt, R., Tagesson, T., & Ehammer, A. (2014). Using earth observation-based dry season NDVI trends for assessment of changes in tree cover in the Sahel. *International Journal of Remote Sensing*, 35(7), 2493–2515.
- Huffman, G. J., Adler, R. F., Bolvin, D. T., Gu, G., Nelkin, E. J., Bowman, K. P., et al. (2007). The TRMM Multisatellite Precipitation Analysis (TMPA): Quasi-global, multi-year, combined-sensor precipitation estimates at fine scales. *Journal of Hydrometeorology*, 8(1), 38–55.
- Hussain, M., Chen, D., Cheng, A., Wei, H., & Stanley, D. (2013). Change detection from remotely sensed images: From pixel-based to object-based approaches. *ISPRS Journal of Photogrammetry and Remote Sensing*, 80, 91–106.
- Immitzer, M., Atzberger, C., & Koukal, T. (2012). Tree species classification with Random forest using very high spatial resolution 8-band worldView-2 satellite data. *Remote Sensing*, 4(9), 2661–2693.
- Irons, J. R., Dwyer, J. L., & Barsi, J. A. (2012). The next landsat satellite: The landsat data continuity mission. *Remote Sensing of Environment*, 122, 11–21.
- Jabar, A. S. A., Sulong, G., & George, L. E. (2014). Survey on gap filling algorithms in Landsat 7 ETM+ images. *Journal of Theoretical and Applied Information Technology*, 63(1), 136–146.
- Karlson, M., Ostwald, M., Reese, H., Sanou, J., Tankoano, B., & Mattsson, E. (2015). Mapping tree canopy cover and aboveground biomass in Sudano-Sahelian woodlands using Landsat 8 and random forest. *Remote Sensing*, 7(8), 10017–10041.
- Kelder, Y., Nielsen, T. T., & Fensholt, R. (2013). The role of methodology and spatio-temporal scale in understanding environmental change in peri-urban Ouagadougou, Burkina Faso. *Remote Sensing*, 5, 1465–1483.
- Kranz, O., Sachs, A., & Lang, S. (2015). Assessment of environmental changes induced by internally displaced person (IDP) camps in the Darfur region, Sudan, based on multitemporal MODIS data. *International Journal of Remote Sensing*, 36(1), 190–210.
- Kruse, F. A., Lefkoff, A. B., Boardman, J. W., Heidebrecht, K. B., Shapiro, A. T., Barloon, J. P., et al. (1993). The spectral image processing system (SIPS) - Interactive visualization and analysis of imaging spectrometer data. *Remote Sensing of Environment*, 44, 145–163.
- Lambin, E. F., Goyvaerts, K., & Petit, C. (2003). Remotely-sensed indicators of burning efficiency of savannah and forest fires. *International Journal of Remote Sensing*, 24(15), 3105–3118.
- Lang, S., Tiede, D., Hölbling, D., Füreder, P., & Zeil, P. (2010). Earth observation (EO)-based ex post assessment of internally displaced person (IDP) camp evolution and population dynamics in Zam Zam, Darfur. *International Journal of Remote Sensing*, 31, 5709–5731.
- Liu, C., Frazier, P., & Kumar, L. (2007). Comparative assessment of the measures of thematic classification accuracy. *Remote Sensing of Environment*, 107, 606–616.
- Liu, J., Heiskanen, J., Aynekulu, E., & Pellikka, P. K. E. (2015). Seasonal variation of land cover classification accuracy of Landsat 8 images in Burkina Faso. *International Archives of the Photogrammetry, Remote Sensing and Spatial Information Sciences - ISPRS Archives*, 40(7W3), 455–460.
- Liu, D., & Xia, F. (2010). Assessing object-based classification: Advantages and limitations. *Remote Sensing Letters*, 1(4), 187–194.
- Lyytinen, E. (2009). *Household energy in refugee and IDP camps: Challenges and solutions for UNHCR. New issues in refugee research*. United Nations High Commissioner for Refugees Research Paper No. 172.
- Maystadt, J.-F. O., Calderone, M., & You, L. (2015). Local warming and violent conflict in North and South Sudan. *Journal of Economic Geography*, 15(3), 649–671.
- Mbow, C., Fensholt, R., Nielsen, T. T., & Rasmussen, K. (2014). Advances in monitoring vegetation and land use dynamics in the Sahel. *Geografisk Tidsskrift*, 114(1), 84–91.
- McElhinny, C., Gibbons, P., Brack, C., & Bauhus, J. (2005). Forest and woodland stand structural complexity: Its definition and measurement. *Forest Ecology and Management*, 218(1–3), 1–24.
- Moeller, M. (2011). Systemvergleich hochauflösender optischer Satellitenfernerkundungssensoren [Comparison of high resolution optical remote sensing satellite sensor systems]. [Angewandte Geoinformatik 2011. Contributions to the 23rd AGIT Symposium] In J. Strobl, T. Blaschke, & G. Griesebner (Eds.). *Angewandte geoinformatik 2011. Beiträge zum 23. AGIT symposium, salzburg* (pp. 1–9). Heidelberg: Wichmann.
- Naidoo, L., Cho, M. A., Mathieu, R., & Asner, G. (2012). Classification of savanna tree species, in the Greater Kruger National Park region, by integrating hyperspectral and LiDAR data in a Random Forest data mining environment. *ISPRS Journal of Photogrammetry and Remote Sensing*, 69, 167–179.
- Ndegwa, G. (2016). *Natural resources management strategy for refugees and host community in Jamjang County*. Juba: UNHCR, Danish Refugee Council, Danish Demining Group.
- Nouri, H., Beecham, S., Anderson, S., & Nagler, P. (2013). High spatial resolution WorldView-2 imagery for mapping NDVI and its relationship to temporal urban landscape evapotranspiration factors. *Remote Sensing*, 6(1), 580–602.
- Oshiek, A. (2015). Conflict and forest resources in Darfur. *Unasylva*, 66(243/244), 62–66 (1–2).
- Pal, M., & Mather, P. M. (2005). Support vector machines for classification in remote sensing. *International Journal of Remote Sensing*, 26(5), 1007–1011.
- Pettorelli, N., Vik, J. O., Mysterud, A., Gaillard, J.-M., Tucker, C. J., & Stenseth, N. C. (2005). Using the satellite-derived NDVI to assess ecological responses to environmental change. *Trends in Ecology & Evolution*, 20(9), 503–510.

- Pontius, R. G., Jr., & Millones, M. (2011). Death to Kappa: Birth of quantity disagreement and allocation disagreement for accuracy assessment. *International Journal of Remote Sensing*, 32(15), 4407–4429.
- Pontius, R. G., Jr., & Santacruz, A. (2014). Quantity, exchange, and shift components of difference in a square contingency table. *International Journal of Remote Sensing*, 35(21), 7543–7554.
- Pu, R., Landry, S., & Zhang, J. (2015). Evaluation of atmospheric correction methods in identifying urban tree species with WorldView-2 imagery. *IEEE Journal of Selected Topics in Applied Earth Observations and Remote Sensing*, 8(5), 1886–1897.
- Raleigh, C., & Urdal, H. (2007). Climate change, environmental degradation and armed conflict. *Political Geography*, 26(6), 674–694.
- Rasmussen, M. O., Göttsche, F.-M., Diop, D., Mbow, C., Olesen, F.-S., Fensholt, R., et al. (2011). Tree survey and allometric models for tiger bush in northern Senegal and comparison with tree parameters derived from high resolution satellite data. *International Journal of Applied Earth Observation and Geoinformation*, 13, 517–527.
- Roberts, J., Tesfamichael, S., Gebreslasie, M., Van Aardt, J., & Ahmed, F. (2007). Forest structural assessment using remote sensing technologies: An overview of the current state of the art. *Southern Hemisphere Forestry Journal*, 69(3), 183–203.
- Salih, A. A. M., Körnich, H., & Tjernström, M. (2013). Climate impact of deforestation over South Sudan in a regional climate model. *International Journal of Climatology*, 33(10), 2362–2375.
- Schneider, A. (2012). Monitoring land cover change in urban and peri-urban areas using dense time stacks of Landsat satellite data and a data mining approach. *Remote Sensing of Environment*, 124, 689–704.
- Sosnowski, A., Ghoneim, E., Burke, J. J., Hines, E., & Halls, J. (2016). Remote regions, remote data: A spatial investigation of precipitation, dynamic land covers, and conflict in the Sudd wetland of South Sudan. *Applied Geography*, 69, 51–64.
- Spröhnle, K., Kranz, O., Schoepfer, E., Moeller, M., & Voigt, S. (2016). Earth observation-based multi-scale impact assessment of internally displaced person (IDP) camps on wood resources in Zalingei, Darfur. *Geocarto International*, 31(5), 575–595.
- Symeonakis, E., & Higginbottom, T. (2014). Bush encroachment monitoring using multi-temporal landsat data and random forests. *International archives of the photogrammetry. Remote Sensing and Spatial Information Sciences - ISPRS Archives*, 40(2), 29–35.
- Thulstrup, A., & Henry, W. J. (2015). Women's access to wood energy during conflict and displacement: Lessons from Yei county, South Sudan. *Unasylva*, 66(243/244), 52–56 (1–2).
- Tiede, D., & Lang, S. (2009). IDP camp evolution analysis in Darfur using VHSR optical satellite image time series and scientific visualization on virtual globes. In H. Guo, & C. Wang (Eds.). *Proceedings of SPIE 7840, sixth international symposium on digital Earth: Models, algorithms, and virtual reality* (pp. 7). Beijing: SPIE.
- Tiller, S., & Healy, S. (2013). Have we lost the ability to respond to refugee crises? The Maban response. *Humanitarian Exchange*, 57, 17–20.
- Tomppo, E., Olsson, H., Ståhl, G., Nilsson, M., Hagner, O., & Katila, M. (2008). Combining national forest inventory field plots and remote sensing data for forest databases. *Remote Sensing of Environment*, 112(5), 1982–1999.
- Tscharntke, T., Clough, Y., Wanger, T. C., Jackson, L., Motzke, I., Perfecto, I., et al. (2012). Global food security, biodiversity conservation and the future of agricultural intensification. *Biological Conservation*, 151(1), 53–59.
- Tucker, C. J. (1979). Red and photographic infrared linear combinations for monitoring vegetation. *Remote Sensing of Environment*, 8(2), 127–150.
- UNEP (United Nations Environment Programme) (2007). *Sudan. Post-conflict environmental assessment*. Nairobi: UNEP.
- UNEP (United Nations Environment Programme) (2009). *From conflict to peacebuilding. The role of natural resources and the environment*. Nairobi: UNEP.
- UNESCO (United Nations Educational, Scientific and Cultural Organization) (2013). *Country programming document. South Sudan 2014 – 2016*. Tongping, Juba, South Sudan: United Nations Educational, Scientific and Cultural Organization.
- UNHCR (United Nations High Commissioner for Refugees) (2014). *Global strategy for safe access to fuel and energy. A UNHCR strategy 2014-2018*. Geneva: UNHCR.
- UNHCR (United Nations High Commissioner for Refugees) (2016). *Global trends. Forced displacement in 2015*. Geneva: UNHCR.
- Urdike, T., & Comp. C. (2010). *Radiometric use of WorldView-2 imagery*. Technical Note: DigitalGlobe®.
- Wu, W., De Pauw, E., & Helldén, U. (2013). Assessing woody biomass in African tropical savannahs by multiscale remote sensing. *International Journal of Remote Sensing*, 34(13), 4525–4549.
- Zeidler, J., Wegmann, M., & Dech, S. (2012). Spatio-temporal robustness of fractional cover upscaling. A Case study in semi-arid Savannah's of Namibia and Western Zambia. *Proceedings of SPIE - the international society for optical engineering: Vol. 8538*, (pp. 85380S–). .
- Zhang, Z., Xu, C.-Y., Yong, B., Hu, J., & Sun, Z. (2012). Understanding the changing characteristics of droughts in Sudan and the corresponding components of the hydrologic cycle. *Journal of Hydrometeorology*, 13(5), 1520–1535.
- Zhu, X., Liu, D., & Chen, J. (2012). A new geostatistical approach for filling gaps in Landsat ETM+ SLC-off images. *Remote Sensing of Environment*, 124, 49–60.